Development of a Piezo-actuated Robot for Cell Injection

D. Chakarov, K. Kostadinov, A. Shulev and T. Tiankov
Institute of Mechanics, Bulgarian Academy of Sciences, Acad. G. Bonchev Str., bl. 4, 1113, Sofia, Bulgaria

Keywords: Parallel Micromanipulator, Piezo-actuator, Elastic Joint, Preliminary Tension, Cell Injection, Simulations, Experimental Investigation.

Abstract: In the presented work model and experiments of compliant robots with piezo actuators are carried out. The robot is designed to perform automatic injection of cells in the range of 10-30 μm. A kinematics model of serial-parallel structures is presented. Pseudo rigid body approach is used, where the elastic joints are modelled as revolute joints. Models for tension of parallel structures with elastic joints are developed in order to eliminate backlashes, to diminish hysteresis, and to improve the performance of the piezo-actuators. Two design approaches are proposed. First approach ensures preliminary tensioning by assembly translation along the axes of the driving joints. Second approach ensures preliminary tensioning by assembly deflections of the basic serial chain elastic joints. The design of new 3-degrees of freedom (DOF) piezo actuated micro-manipulators with serial-parallel structure including elastic joints capable of performing cell injection is presented. Numerical experiments are done for tensioning of the manipulator. An estimation of the manipulator mechanical parameters for different approaches is carried out. Manipulator simulations with elastic joints are performed using FEA based function of a CAD system. The real manipulator prototype is experimentally investigated using digital image correlation technique.

1 INTRODUCTION

Micro- and nano- robots have emerged as an important technological advancement in the last 15 years. The significance of this advancement is highlighted in many applications where positioning of components within micrometer or nanometre accuracy is required. Micro- and nano- robots are mostly used in biological and microelectronics researches, cellular technology, chemistry, electro-chemical impedance technique and investigation of thin films, in atomic force microscopes and scanning tunnelling microscopes.

The body of these micromanipulators is constituted of a high-precision mechanical structure which is free from backlash, friction and hysteresis in order to obtain the required sub-micron accuracy (Kasper, 2004; Pernette, 1997).

As well known, parallel kinematic mechanisms possess inherent advantages over conventional serial manipulators, such as high levels of rigidity, load capacity, velocity, precision, etc. However, traditional parallel manipulators suffer from errors due to backlash, hysteresis, and manufacturing defects in the joints, as for any mechanical systems composed of conventional joint. Hence, it is a major challenge to achieve ultrahigh precision with conventional joints.

On the other hand, compliant mechanisms, i.e., flexure-based mechanisms can be utilized into parallel mechanisms for high precision applications (Yong, 2008) because the compliant mechanisms have many advantages in terms of vacuum compatibility, absence of backlash and non-linear friction, simple structure and manufacturing simplicity. Compliant mechanisms generate their motions through elastic deformation. These mechanisms use flexure hinges to replace the joints in a rigid-link mechanisms, thus avoiding the use of moving and sliding joints.

Many actuation principles have been applied to drive the compliant mechanism in a micro and nano-robots. Piezoelectric actuators, electrostatic, electro-magnetic and shape memory alloy actuators have been utilised to provide fine motions of the micro- and nanorobots. Piezoelectric actuators are used commonly to provide fine resolution of input displacements in the sub-nanometre range (Chih-Liang Chu, 2006), since their resolution is dependent solely on the quality of applied voltage signal. As

Chakarov D., Kostadinov K., Shulev A. and Tiankov T..
Development of a Piezo-actuated Robot for Cell Injection.
DOI: 10.5220/0003984700210030
In *Proceedings of the 9th International Conference on Informatics in Control, Automation and Robotics* (ICINCO-2012), pages 21-30
ISBN: 978-989-8565-22-8
Copyright © 2012 SCITEPRESS (Science and Technology Publications, Lda.)

the presence of unwanted transverse loads may damage some types of motors such as piezoelectric actuators, the concept of totally decoupling is accepted to isolate/protect the actuators. To eliminate the cross-axes coupling errors between the axes translations in compliant parallel stages, design of a totally decoupled parallel micro positioning stages is proposed (Li Y., 2011).

The pseudo-rigid-body-model is commonly used (Zhang, 2002), in order to predict the displacements of compliant mechanisms with elastic joints. As a rule, it models an elastic joint as a revolute joint with a torsion spring attached. The pseudo-rigid-body method is effective and it simplifies the model of compliant mechanisms. An analytical model is created out taking into account compliances of elastic joints in all axes to estimate the mechanism stiffness with elastic joints. The analytical model describes the relationship between input and output displacements of the mechanism (Pham, 2005).

Different ways exist for the computation of the stiffness of the elastic joints or of the whole manipulator. One of them is Finite Element Analysis (FEA) (Yong, 2008). The FEA method is provided to be the most accurate and reliable, since the joints are modelled with their true dimensions and shapes. Disadvantage of this method is its high computational expenses.

In recent years, many attempts have been made to leverage robotic technologies to facilitate the process of cell injection (Lu, 2011). Large effort has been made to integrate robotics technology into micro-manipulation platform that has substantial biological relevance (Tang, 2012).

The aim of this work is to create pseudo rigid body model of closed structures with elastic joints for micro- and nano- manipulations and to develop approaches for tension of closed structures with piezo-actuators. We designed a robot possessing serial-parallel structures capable of automatic cell injection realization. We performed numeric experimentation and estimation of the build up models and approaches as well as experimental investigation of the prototyped robotic system.

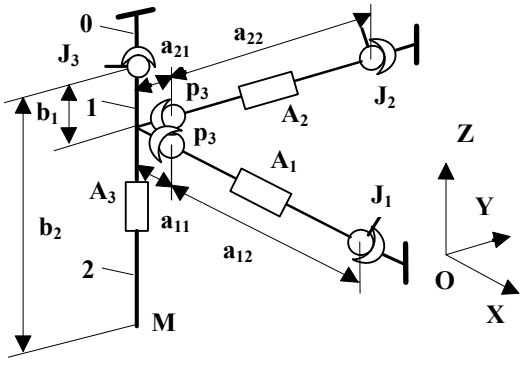

Figure 1: Kinematics scheme of serial-parallel manipulator with 3 DOF.

2 PSEUDO-RIGID-BODY MODEL AND MODEL OF PRELIMINARY TENSIONING OF A PARALLEL STRUCTURE WITH ELASTIC JOINTS

The studied micro-manipulator is a component of a robot capable of performing automatic cell injection. The aim of the micro-manipulator is to orientate and to position the pipette according to the cells, as well as to perform the necessary motions for cell injection. The micro manipulator with a serial-parallel structure is selected as shown in Fig. 1.

Here, pseudo rigid body model is used in order to describe the compliant micromanipulator (Chakarov, 2009). It models all links as rigid bodies and the elastic joints as revolute joints. Each 2 DOF elastic joints are replaced by a 2 DOF universal joint with torsion stiffness, as shown in Fig. 1.

Base 0, manipulator body 1, actuator A_3 with working tool 2 and end- effector M form a serial chain. The body 1 is linked with the base 0 by means of 2 DOF universal joints J_3. Actuators A_1 and A_2 are linked with the base 0 by means of 2 DOF universal joints J_1 and J_2, thus forming parallel chains. The actuators are fixed to the body 1 via two kinematics joints, which are 3 DOF spherical joints (P3). Actuators A_1 and A_2 are modelled as 1 DOF prismatic joints and the number DOF of the structure come out to be h=3.

According to this model, generalized parameters are accepted to be the parameters of the relative motions in all joints of the structure - elastic and non-elastic, presented by the vectors:

$$\mathbf{q} = [q_1, q_2, q_3]^T, \quad (1)$$

a vector of the generalized coordinates in the joints of the main serial chain with 3 DOF,

$$\mathbf{w} = [w_{11}, w_{12}, w_{21}, w_{22}]^T, \quad (2)$$

a vector of coordinates in the passive universal joints J_1, J_2 of the parallel chains, and

$$\mathbf{l} = [l_1, l_2, l_3]^T, \quad (3)$$

a vector of coordinates in the actuator joints A_1,A_2, and A_3.

Let the linear coordinates of the end-effector M are denoted as:

$$\mathbf{X} = [\mathbf{X_1}, \mathbf{X_2}, \mathbf{X_3}]^T . \quad (4)$$

The relation between the parameters of the basic serial chain (1) and the parameters of the end-effector (4) is known as a direct kinematics problem for the serial chain $\mathbf{X = \Psi(q)}$. This problem on the level of velocities is presented by the equations:

$$\dot{\mathbf{X}} = \mathbf{J}\dot{\mathbf{q}} , \quad (5)$$

where $\mathbf{J} = [\partial \mathbf{X}/\partial \mathbf{q}]$ is the (3 x 3) matrix of Jacoby.

In the parallel structure, each closed loop implies the appearance of a connection between the generalized parameters (1), (2), (3). These connections are expressed by 6 scalar functions for the structure including 2 parallel loops: $\mathbf{\Psi_i(q, w, l) = 0,}$ i=1,…,6. The differentiation of the above equations, gives the matrix of partial derivations $\mathbf{W} = \partial \mathbf{w}/\partial \mathbf{q}$ and $\mathbf{L} = \partial \mathbf{l}/\partial \mathbf{q}$ with size (4 x 3) and (3 x 3) and the relations between generalized velocities:

$$\dot{\mathbf{w}} = \mathbf{W}\dot{\mathbf{q}} \quad (6)$$

$$\dot{\mathbf{l}} = \mathbf{L}\dot{\mathbf{q}} \quad (7)$$

As the number of parameters (3) is equal to the DOF h=3, these parameters can be selected as independent ones. In equation (7) we have the inverse relation:

$$\dot{\mathbf{q}} = \mathbf{L}^{-1}\dot{\mathbf{l}} . \quad (8)$$

Equations (5) and (8) allow determining the end-effector velocities, while equations (6) and (8) - the velocities of passive joints, as a function of the velocities of the linear actuator joints $\dot{\mathbf{l}}$:

$$\dot{\mathbf{X}} = \mathbf{J}\mathbf{L}^{-1}\dot{\mathbf{l}} \quad \text{and} \quad (9)$$

$$\dot{\mathbf{w}} = \mathbf{W}\mathbf{L}^{-1}\dot{\mathbf{l}} . \quad (10)$$

The displacements of the piezo-actuators are small as compared to the link lengths. Therefore, the micro-manipulator is almost configurationally invariant and its matrix of partial derivations **J, L** and **W** are assumed to be constants (Zhang, 2002). The equations (8), (9), (10) give the relations between the small displacements of the micro actuators δl, the joints of the main serial chain **δq,** the end-effector **δX** and the passive joints **δw**:

$$\delta\mathbf{q} = \mathbf{L}^{-1}\delta\mathbf{l} , \quad (11)$$

$$\delta\mathbf{X} = \mathbf{J}\mathbf{L}^{-1}\delta\mathbf{l} \quad \text{and} \quad (12)$$

$$\delta\mathbf{w} = \mathbf{W}\mathbf{L}^{-1}\delta\mathbf{l} . \quad (13)$$

A preliminary tensioning of the mechanical micro-manipulation system is necessary in order to eliminate the backlash of the kinematics joints and to improve the performance of the piezo-actuators. It is possible to use deformation in elastic joints to achieve tension in closed structures resulting in restoring forces. The following two approaches can be used for tensioning of the manipulator:

1) Preliminary tensioning by means of assembly translation along the axes of the linear driving joints, which leads to deflection in all the system joints and to tensioning of the actuators with a force $\mathbf{F_1}$.

2) Preliminary tensioning by assembly deflections of the basic serial chain elastic joints, which leads to deflection only in these joints and to tensioning of the actuators with a force $\mathbf{F_1}$.

2.1 Model of Preliminary Tensioning by Assembly Translation along the Axes of the Driving Joints

The assembly displacement along the axes of the driving joints denoted by the vector $\mathbf{\Delta l_0}$ leads to deflection in all the system joints, appearance of resistant forces in the elastic joints and tensioning of the actuators along their axis by force $\mathbf{F_1}$. The assembly displacement leads to elastic deformations in the driving joints denoted by the vector $\mathbf{\Delta l_1}$. The assembly displacements $\mathbf{\Delta l_0}$ along the axes of the drives and the working shifts of the drives $\mathbf{\Delta l_2}$ are combined in the vector:

$$\Delta\mathbf{l} = \Delta\mathbf{l}_0 + \Delta\mathbf{l}_2 . \quad (14)$$

The resultant displacement along the axes of the driving joints after tensioning is equal to the sum:

$$\delta\mathbf{l} = \Delta\mathbf{l} - \Delta\mathbf{l}_1 . \quad (15)$$

This displacement is defined according to (11) by means of deflections in the joins of the main serial chain $\delta\mathbf{q}$. The deflections of the end-effector $\delta\mathbf{X}$ according to (12) and the deflections in the elastic joints of the parallel chains $\delta\mathbf{w}$ according to (13) are dependent on the resulting displacement along the axes of the driving joints also (15).

The elastic deformations in the driving joints $\mathbf{\Delta l_1}$ define the resistant forces in them:

SCITEPRESS SCIENCE AND TECHNOLOGY PUBLICATIONS

$$\mathbf{F_l} = \mathbf{K_l}\Delta\mathbf{l}_1 . \quad (16)$$

The resulting displacements in the driving joints (15) with the help of (13) define the resistant forces in the elastic joins of the parallel chains:

$$\mathbf{F_w} = \mathbf{K_w}\delta\mathbf{w} , \quad (17)$$

and with the help of (11) define the resistant forces in the elastic joints of the main chain:

$$\mathbf{F_q} = \mathbf{K_q}\delta\mathbf{q} . \quad (18)$$

$\mathbf{K_l}$, $\mathbf{K_w}$ and $\mathbf{K_q}$ above**,** are the matrixes of the axial stiffness in the driving joints, in the elastic joints of the parallel chains and in the elastic joints of the main chain, respectively.

The elastic forces after system tensioning establish static equilibrium:

$$\mathbf{F_q} + \mathbf{W}^{\mathbf{T}}\mathbf{F_w} = \mathbf{L}^{\mathbf{T}}\mathbf{F_l} \quad (19)$$

which according to (18), (17), (11), (13) and (15) is defined by the equality:

$$\mathbf{K_q}\mathbf{L}^{-1}[\Delta\mathbf{l} - \Delta\mathbf{l}_1] + \mathbf{W}^{\mathbf{T}}\mathbf{K_w}\mathbf{W}\mathbf{L}^{-1}[\Delta\mathbf{l} - \Delta\mathbf{l}_1] = \mathbf{L}^{\mathbf{T}}\mathbf{F_l} \quad (20)$$

After considering the inverse form of (16):

$$\Delta\mathbf{l}_1 = \mathbf{K_l}^{-1}\mathbf{F_l} \quad (21)$$

and modification of the above equality, the displacements along the axes of the actuators are defined as a function of the actuators forces:

$$\Delta\mathbf{l} = [\mathbf{L}[\mathbf{K_q} + \mathbf{W}^{\mathbf{T}}\mathbf{K_w}\mathbf{W}]^{-1}\mathbf{L}^{\mathbf{T}} + \mathbf{K_l}^{-1}]\mathbf{F_l} , \quad (22)$$

where:

$$\mathbf{L}[\mathbf{K_q} + \mathbf{W}^{\mathbf{T}}\mathbf{K_w}\mathbf{W}]^{-1}\mathbf{L}^{\mathbf{T}} + \mathbf{K_l}^{-1} = \mathbf{B_l} \quad (23)$$

is the adduced system compliance to actuator axes. The desired tensioning force $\mathbf{F_{l0}}$ defines according to (22) and (14) the necessary assembly displacement along the axes of the driving joints $\mathbf{\Delta l_0 = \Delta l}$**,** when the actuators are not active **($\mathbf{\Delta l_2 = 0}$).** The actuators driving shifts $\mathbf{\Delta l_2}$ after system tensioning with displacement $\mathbf{\Delta l_0}$ lead to a force variation of the actuators $\mathbf{F_{l0}}$ with the value of $\mathbf{F_{l2}}$ defined by (22):

$$\Delta\mathbf{l}_0 + \Delta\mathbf{l}_2 = \mathbf{B_l}[\mathbf{F_{l0}} + \mathbf{F_{l2}}] . \quad (24)$$

The end-effector varies after manipulator tensioning according to equalities (12), (15) and (14):

$$\delta\mathbf{X} = \mathbf{J}\mathbf{L}^{-1}[\Delta\mathbf{l}_0 + \Delta\mathbf{l}_2 - \Delta\mathbf{l}_1] , \quad (25)$$

where

$$\Delta\mathbf{l}_1 = \mathbf{K_l}^{-1}[\mathbf{F_{l0}} + \mathbf{F_{l2}}] . \quad (26)$$

2.2 Model of Preliminary Tensioning by Assembly Deflections of the Basic Serial Chain Elastic Joints

The assembly displacement along the axes of the elastic joints of the basic serial chain denoted by the vector $\mathbf{\Delta q_0}$ leads to a deflection in all the system joints, appearance of resisting forces in the elastic joints and tensioning of the actuators along their axes with a force $\mathbf{F_1}$. The raising elastic deformations in the driving joints are denoted as in the previous case with $\mathbf{\Delta l_1}$**,** the working shifts of the actuators - with $\mathbf{\Delta l_2}$ and then the resultant displacements along the axes of the driving joints are equal to the sum:

$$\delta\mathbf{l} = \Delta\mathbf{l}_2 - \Delta\mathbf{l}_1 . \quad (27)$$

These displacements lead to additional deformations in the joints of the base chain according to (11).The resultant joint displacements of the base chain after their tensioning by the deformations $\mathbf{\Delta q_0}$ are:

$$\Delta\mathbf{q} = \Delta\mathbf{q}_0 + \delta\mathbf{q} . \quad (28)$$

The resistant torques which arise in the elastic joints of the basic chain are defined by their stiffness $\mathbf{K_q}$ and deformations according to (28), (11) and (27):

$$\mathbf{F_q} = \mathbf{K_q}[\Delta\mathbf{q}_0 + \mathbf{L}^{-1}[\Delta\mathbf{l}_2 - \Delta\mathbf{l}_1]] . \quad (29)$$

The resistant forces in the elastic joints of the parallel chains are derived in the same way as in the previous case according to equality (17) where the equalities (13) and (27) are also valid. The static system equilibrium (19) established after taking into account (29) and (17) is defined by the value:

$$\begin{aligned} &\mathbf{K_q}[\Delta\mathbf{q}_0 + \mathbf{L}^{-1}[\Delta\mathbf{l}_2 - \Delta\mathbf{l}_1]] + \\ &\mathbf{W}^{\mathbf{T}}\mathbf{K_w}\mathbf{W}\mathbf{L}^{-1}[\Delta\mathbf{l}_2 - \Delta\mathbf{l}_1] = \mathbf{L}^{\mathbf{T}}\mathbf{F_l} \end{aligned} \quad (30)$$

The upper equality allows definition of the pre-tensioning in the basic joints, after taking into account the dependence of the deformations in the driving joints on the value of the driving forces (21):

$$\begin{aligned} &\Delta\mathbf{q}_0 = \\ &-\mathbf{K_q}^{-1}[\mathbf{W}^{\mathbf{T}}\mathbf{K_w}\mathbf{W}\mathbf{L}^{-1}[\Delta\mathbf{l}_2 - \mathbf{K_l}^{-1}\mathbf{F_l}] - \mathbf{L}^{\mathbf{T}}\mathbf{F_l}] \\ &-\mathbf{L}^{-1}[\Delta\mathbf{l}_2 - \mathbf{K_l}^{-1}\mathbf{F_l}] \end{aligned} \quad (31)$$

The desired tensioning force of the actuators $\mathbf{F_{l0}}$**,** when they are not active **($\mathbf{\Delta l_2 = 0}$),** defines according to (31) the necessary assembly displacement along the axes of the elastic joints of the basic serial chain $\mathbf{\Delta q_0}$. The working actuator shifts $\mathbf{\Delta l_2}$ after system

SCITEPRESS SCIENCE AND TECHNOLOGY PUBLICATIONS

tensioning lead to force variation of the actuators which according to (31) is defined by the equality:

$$\mathbf{F_l} = [[\mathbf{K_q} + \mathbf{W^T K_w W}]\mathbf{L}^{-1}\mathbf{K_l}^{-1} + \mathbf{L^T}]^{-1} * [\mathbf{K_q}\Delta\mathbf{q}_0 + [\mathbf{K_q} + \mathbf{W^T K_w W}]\mathbf{L}^{-1}\Delta\mathbf{l}_2] \quad (32)$$

The end-effector position varies at manipulator tensioning and at performing of the work shift according to the equalities (12), (27):

$$\delta\mathbf{X} = \mathbf{J}\mathbf{L}^{-1}[\Delta\mathbf{l}_2 - \Delta\mathbf{l}_1] \quad . \quad (33)$$

The raising elastic deformations in the driving joints above are defined according to (21) and (32).

3 DESIGN AND NUMERICAL EXPERIMENTATION OF THE MICRO-MANIPULATOR

3.1 Design of a Robot System for Cell Injection

A robot has been designed to perform automatic cell injection (Kostadinov, 2009). The robot system includes a macro-manipulator and a local micro-manipulator. The macro-manipulator is scheduled to insert the micro-manipulator with the injection pipette in hand in the working zone. Here, the biological cells on the range of 10-30 [μm] are preliminary positioned in a matrix feeder. The aim of the micro-manipulator is to orientate and to position the pipette according to the cells, as well as to perform the injection motions. The micro-manipulator is designed as it is shown in the simulation in Fig. 2. The manipulator body 1 is linked to the base body 0 by means of an elastic joint J_3 forming a serial chain. Actuators A_1 and A_2 are located perpendicularly to the body 1 and they are linked to the base 0 by means of elastic joints J_1 and J_2, thus forming parallel chains. The actuators are fixed to the body 1 via spherical joints. Parallel structure comprising actuators A_1 and A_2 performs orientation motions, while the actuator A_3 performs injection through the pipette 2 attached to it. Piezoelectric stack actuators are chosen, hereafter called piezo-actuators, for their smooth motion, high accuracy, and fast response.

The joints J_1, J_2 and J_3 are recognized as double notched elastic beam joints. These joints allow by means of a preliminary deformation to achieve pre-tension of the piezo-actuators. The joint geometry shown in Fig. 3 is accomplished with the help of electro-discharge machining. This geometry allows the desired low stiffness to be achieved in two transverse mutually perpendicular directions of bending and high stiffness in the rest non-motional direction.

The main dimensions of the studied manipulator according to Fig.1 are $a_{12}=a_{22}=0.066$[m], $a_{11}=a_{21}=0.007$[m], $b_1=0.030$[m], $b_2=0.180$[m]. The travel of the piezo-actuators used is as follow: actuator A_3:60 10^{-6}[m]; actuators A_1, A_2: 30 10^{-6}[m]. The actuators possess axial stiffness 27 10^6 [N/m] and pushing force capacity 1000 [N]. The torque limits of the actuators are 0.35 [N/m].

Forces $\mathbf{F_l}$ in the driving joints which tension axially the actuators $A_1$and A_2 are defined by the stiffness of the elastic joints $\mathbf{J_3}$ and $\mathbf{J_1}$, $\mathbf{J_2}$ and by the preliminary deflections according to the mentioned above approaches.

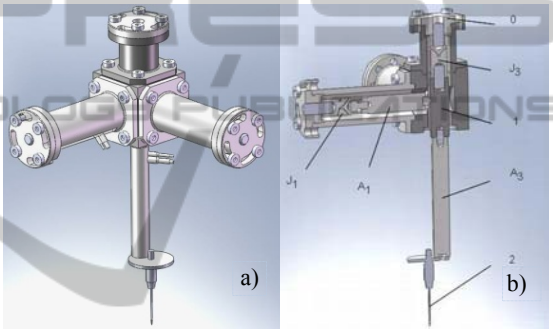

Figure 2: Micro-manipulator: a) general view; b) cross section. (0-base; 1 – coupling body; 2: glass pipette; A_1-A_3 – piezo actuators; J_1, J_3 – elastic joints).

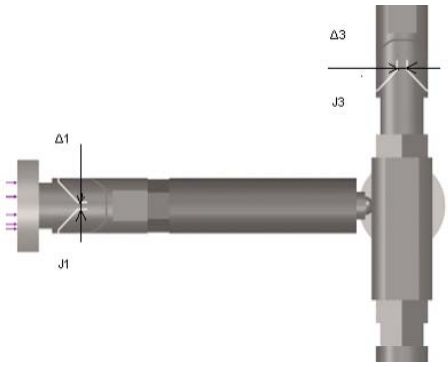

Figure 3: Joints J_1 and J_3 performed as double notched elastic beam joints.

The joint geometry presented in Fig. 3 allows the desired angular stiffness to be achieved by means of the width Δ variation of the most bending loaded area. An assessment of the realized stiffness is performed using FEA-based technique, applied to the entire elastic system.

The selected material of the elastic joint is stainless steel (X2CrNi18-9) with Young's modulus E = 190 [GPa] and Yield strength σ=0.465 [GPa]. Joints J_1, J_2 are selected with $\Delta_1 = \Delta_2 = 0.0012$ [m] and joint J_3 with $\Delta_3 = 0.0020$ [m] in developing manipulator.

In result of the assessment, the value of join angular stiffness is 91.3 [Nm/rad] for joints J_1, J_2 and 340.3 [Nm/rad] for joint J_3. The angular stiffness matrices are defined as:

$$K_q = \mathrm{diag}[340.3; 340.3; 0][\mathrm{Nm/rad}]; \quad (34)$$

$$K_w = \mathrm{diag}[91.3; 91.3; 91.3; 91.3][\mathrm{Nm/rad}]. \quad (35)$$

The linear stiffness matrix of actuators is defined as:

$$K_l = \mathrm{diag}[27; 27; 0]10^6\ [\mathrm{N/m}]. \quad (36)$$

3.2 Numeric Experimentation

The matrix of partial derivations **J, L** and **W,** with size (3x3), (3x3) and (4x3) are assumed to be constant according the pseudo-rigid-body-model of serial-parallel structures build up as presented in chapter 2. A software application based on the matrix equalities (11), (12), (13) and (19) is developed to carry out numerical experiments. Experiments are conducted of the preliminary joint deflections for manipulator tensioning according to the presented in chapter 2 approaches.

3.2.1 Mechanical Micro-manipulation System Preliminary tensed According to Approach 1

The value of forces in the driving joints is selected to be 10% from the push force capacity of the actuators used or 100 [N]. The vector of desired actuator forces is defined as:

$$F_{l0} = [-100; -100; 0]^T[\mathrm{N}]. \quad (37)$$

Experiments are carried out when tension forces are presented by vector (37), the stiffness of the elastic joint J_3 is presented by matrix (34), the stiffness of the elastic joints J_1, J_2 - by matrix (35) and the stiffness of piezo-actuators A_1, A_2 - by matrix (36).

Desired assembly deflection in the driving joints, which leads to deflection in all the system joints and to tension of the actuators with a force 100 **[N]** according to (22) is:

$$\Delta l_0 = [-256.704; -256.707; 0]^T 10^{-6}[\mathrm{m}]. \quad (38)$$

Deformations Δl_1 in the driving joints as a result of the piezo-actuators' compliance, shown by the matrix (36), is defined by the equality (21):

$$\Delta l_1 = [-3.703; -3.703; 0]^T 10^{-6}[\mathrm{m}]. \quad (39)$$

Equation (15) allows determination of the effective motion in the driving joints, shown below:

$$\delta l = [-253.001; -253.001; 0]^T 10^{-6}[\mathrm{m}]. \quad (40)$$

According to (12) and giving an account of (40), the deflections of the end-effector are:

$$\Delta X = [-1518.006; -1518.006; 0]^{-T}\ 10^{-6}\ [\mathrm{m}]. \quad (41)$$

For the effective motion in the driving joints (40) and selected angular stiffness, the torques of the elastic joints J_3 and J_1, J_2 according (11), (18) and (13), (17) possess values:

$$F_q = [-2.869; 2.869; 0]^T\ [\mathrm{Nm}], \quad (42)$$

$$F_w = [0.316; 0; -0.316; 0]^T\ [\mathrm{Nm}]. \quad (43)$$

Torques (43) of the elastic joints J_1, J_2 lead to undesirable bending loading of the linear piezo-actuators, but they are close to the torque limit of the actuators 0.35 [N/m].

The tensioning force (37) varies at the working shifts of the actuators in a manipulator tension state according to (24). When maximal actuator shifts are presented by the vector:

$$\Delta l_2 = [-30; -30; 0]^T 10^{-6}[\mathrm{m}]. \quad (44)$$

Following (38) and (14), the actuator deflections are:

$$\Delta l = [-286.704; -286.704; 0]^T 10^{-6}[\mathrm{m}]. \quad (45)$$

The already changed tensioning force at maximal actuator shifts according (24) is defined by the vector:

$$F_{l0} + F_{l2} = [-111.686; -111.686; 0]^T[\mathrm{N}]. \quad (46)$$

The effective shifts in the driving joints according to (26) and (15) and the effective shift of the end-effector according to (25) are:

$$\delta l = [-282.568; -282.568; 0]^T 10^{-6}[\mathrm{m}] \quad (47)$$

$$\delta X = [-1695.408; -1695.408; 0]^T\ 10^{-6}[\mathrm{m}]. \quad (48)$$

The difference **χ** between displacements (41) and (48) forms the working range of the micro-manipulator:

SCITEPRESS SCIENCE AND TECHNOLOGY PUBLICATIONS

$$\chi = [177.402;177.402;60]^T 10^{-6}[\text{m}]. \quad (49)$$

3.2.2 Mechanical Micro-manipulation System Preliminary tensed According to Approach 2

Like the above case, experiments are carried out when tension forces are presented by vector (37), the stiffness of the elastic joint J_3 is presented by matrix (34), the stiffness of the elastic joints J_1, J_2 by matrix (35) and the stiffness of piezo-actuators A_1, A_2 by matrix (36).

The preliminary displacements in the joints of the basic chain, for actuator tensioning when they are at starting position (Δl_2=0), are defined by (31):

$$\Delta q_0 = [-8.944;8.944;0]^T 10^{-3}[\text{rad}]. \quad (50)$$

In the tensioned actuators elastic deformations arise according as (21), which following (27) are equal to:

$$\delta l = [3.703;3.703;0]^T 10^{-6}[\text{m}]; \quad (51)$$

and according as (12) define the deflections of the end effector after tensioning of the actuators:

$$\delta X = [22.218;22.218;0]^{-T} 10^{-6}[\text{m}]. \quad (52)$$

The resistance torque in the elastic joint of the basic chain after the system tensioning defined by (29) is:

$$F_q = [-3.002;3.002;0]^T [\text{Nm}]. \quad (53)$$

When manipulator in a tensioned state performs the maximal shifts of the actuator (44), the driving forces change according to (32) and they are:

$$F_l = [-111.686;-111.686;0]^T [\text{N}]. \quad (54)$$

Elastic deformations of the actuators according to (21) and (54) are:

$$\Delta l_1 = [4.136;4.136;0]^T 10^{-6}[\text{m}]. \quad (55)$$

The resultant displacement along the axes of the drives according to (27) is:

$$\delta \mathbf{l} = [-25.864;-25.864;0]^{\mathbf{T}} 10^{-6}[\text{m}] \quad (56)$$

and the end-effector position according (12) is:

$$\delta X = [-155.184;-155.184;0]^{-T} 10^{-6}[\text{m}]. \quad (57)$$

The difference χ between positions (52) and (57) forms the working range of the micro-manipulator:

$$\chi = [177.402;177.402;60]^T 10^{-6}[\text{m}] \quad (58)$$

The performed experiments show that after system tensioning deflections arise from the starting position of the end-effector and at the first approach these deflections are considerable (41), while at the second one they are smaller (52). The end-effector effective displacements at the same shifts of the actuators in both approaches are equal (49 and 58).

3.3 FEA Simulations

An additional experiment of the static load by actuator tensioning was carried out using FEA modelling as a function of a CAD system. Simulations were conducted when tension forces are attached at the end of motor loop A_1, J_1 and A_2, J_2, respectively. Each motor loop is restricted at the end as linear joints. All the system bodies are simulated by means of the presented above material - X2CrNi18-9, and the stack piezo-actuators are modelled as an elastic joint possessing an axial stiffness 27 10^6[N/m]. The screen with the carried out simulations is shown in Fig. 4.

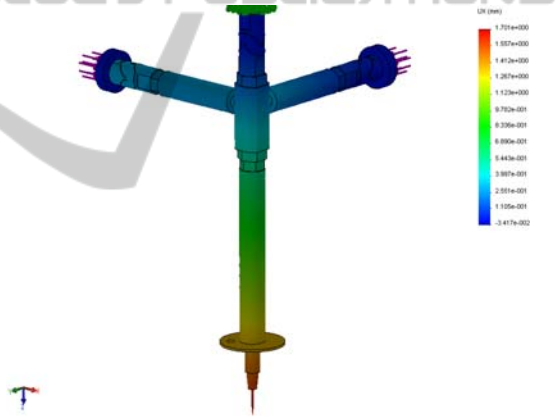

Figure 4: Screen with effective displacements in X direction.

3.3.1 Mechanical Micro-manipulation System Preliminary tensed According to Approach 1

The first experiment is carried out when the tension forces have the values F_{11} =-100 [N] and F_{12}=-100 [N]. Effective displacements at the end point of the end-effector δx and δy were reported by the CAD system, respectively in X and Y direction as it is shown in Table 1. The pointed out results are averaged values from several simulations. Effective displacement δz in Z direction are very small (in submicron range) and they are not object of the present stuffy. Second experiment is carried out when the tension forces have the values F_{11} =-

SCITEPRESS SCIENCE AND TECHNOLOGY PUBLICATIONS

111.686 [N] and F_{12}=-111.686 [N].

The difference χ between end-effector displacements in the two shown above cases define the working range of the micromanipulator in X and Y direction χ_x=184.10^{-6} [m] and χ_y=181.10^{-6} [m]. In the third experiment tension forces have the values F_{11} =-100 [N] and F_{12}=-111.686[N]. Comparing the last result with CAD results obtained one give difference between end-effector displacements in X and Y direction χ_x=6.10^{-6} [m] and χ_y=175.10^{-6} [m] as it is shown in Table 1. The derived results show very close parameter values to those calculated in chapter 3.2.1. We can conclude that because of axis coupling, each of the actuators A_1, A_2 influences the displacements of both axes (X and Y). For example, the displacement of X and Y direction in the second experiment have a difference in the range of 3 μm and displacement of Y direction and effective displacement of X direction in the third experiment, has a disturbance in a range of 6 μm.

Table 1: Effective displacements at the end-effector (1).

	F_{11} =-100[N] F_{12}=-100 [N]	F_{11} =-111.686[N] F_{12}=-111.686 [N]	χ [m]
δx [m]	-1517.10^{-6}	-1701.10^{-6}	184.10^{-6}
δy [m]	-1518.10^{-6}	-1699.10^{-6}	181.10^{-6}
	F_{11} =-100 F_{12}=-100	F_{11} =-100 F_{12}=-111	
δx [m]	-1517.10^{-6}	-1523 10^{-6}	6.10^{-6}
δy [m]	-1518.10^{-6}	-1693 10^{-6}	175.10^{-6}

3.3.2 Mechanical Micro-manipulation System Preliminary tensed According to Approach 2

In this case the preliminary tensioning in the elastic joints of the basic chain is presented with torques (53) attached to the body 1 of the basic chain near to the joint J_3. Actuator loads are presented with forces attached at the end of motor loop A_1, J_1 and A_2, J_2, respectively, similar to the experiments carried out in the previous section, as shown in Fig. 4. Simulations were conducted at values of the actuator forces -100[N] or -111.686[N], similar to the previous experiments. Effective displacements at the end point of the end-effector δx and δy in X and Y direction and difference χ between displacements are shown in Table 2. The derived results show very close parameter values with those calculated in chapter 3.2.2. In this case, as well as in the previous one, the simulations consider influence of each actuator on the displacements along both axes (X and Y), but this influence is smaller as the deflections reach 2-3 μm.

Table 2: Effective displacements at the end-effector (2).

	F_{11} =-100 F_{12}=-100 [N]	F_{11}=-111.686 F_{12}=-111.686 [N]	χ [m]
δx[m]	23.2 10^{-6}	-155.1 10^{-6}	178.3 10^{-6}
δy[m]	25.0 10^{-6}	-155.7 10^{-6}	180.7 10^{-6}
	F_{11} =-100 F_{12}=-100	F_{11} =-100 F_{12}=-111	
δx[m]	23.2 10^{-6}	25.4 10^{-6}	2.2 10^{-6}
δy[m]	25.0 10^{-6}	-154.7 10^{-6}	179.7 10^{-6}

4 EXPERIMENTAL SET-UP & RESULTS

Some experiments proving the functionality of the prototyped micromanipulator (Fig.5.) are performed. An experimental set-up, consisting of an optical system and a translational stage with 3 DOF, has been built up (Fig. 6), to investigate the micro-manipulator. The translational stage is used for precise alignment of the micro-manipulator with respect to the optical system and the image space calibration. It contains 3 orthogonal translational modules (M1÷M3) with integrated linear positioning sensors possessing resolution of 0.1 μm. The micro-manipulator is fixed to the translational stage allowing precise positioning of its end-effector in the image space of the optical system.

This optical system consists of a zoom imaging lens with magnification of 2.5x - 10x at a constant working distance of 35 mm. The camera sensor is CMOS with 2592×1944 pixels and the pixel dimensions are 2.2×2.2 μm^2. The frame rate at full resolution is 3 frames per second (fps) and at VGA – 30 fps. It defines how many times per second we can inspect the system. This parameter together with the computational power and the algorithm effectiveness define the vision control speed (Liu, 2006). If we have efficient numerical algorithms and fast computer system, the vision control is limited only by the camera frame rate (Jin, 2005). The used digital image correlation technique shows that the minimal displacement resolution obtained experimentally is 50 nm (Shulev, 2011).

The first approach for manipulator tensioning is experimented. Each piezo-actuated axis of the micromanipulator was tested separately, thus investigating the working space of the manipulator. The obtained result for axis X actuated by piezo-actuators A1 is presented in Fig. 7. Results show the motion range along the axes X and Y, i.e.: χ_x= χ_y= 226 μm. The result is determined by the used glass pipette length. To measure repeatability, the piezo-

Figure 5: Prototype of micromanipulator with 3 DOF.

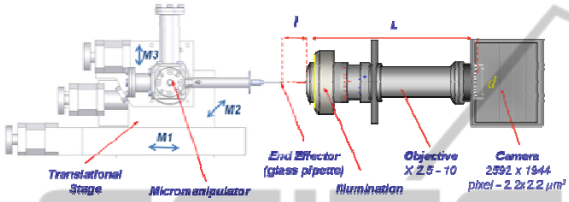

Figure 6: Scheme of the experimental set-up.

actuators with open loop control have been set at a given position 200 times and the end-effector position was measured. Experiments are conducted separately for manipulator tensed according approach 1 and approach 2 and without hysteresis compensation. The obtained results for both approaches are shown in Fig. 8 a) and b). The working shifts of the actuators A1 and A2 are given equal to 1µm. It was found that end-effector maximal positioning error is in a range of (3-5) µm for approach 1 and (0-1) µm for approach 2.

5 CONCLUSIONS

In this paper a model and experiments of compliant robots with piezo-actuators for micro- and nano-manipulations are presented. A kinematics model of serial-parallel structures is presented. Pseudo rigid body approach is used, where the elastic joints are modelled as revolute joints.

Methods for tension of serial-parallel structures with elastic joints are developed in order to eliminate backlashes, to diminish hysteresis, and to improve the performance of the piezo-actuators.

Two design approaches are proposed. First approach ensures preliminary tensioning by assembly translation along the axes of the driving joints. Second approach ensures preliminary tensioning by assembly deflections of the basic serial chain elastic joints.

The new 3 DOF piezo-actuated micro-manipulator designed to perform cell injection is presented. Numerical experiments are done for the manipulator tensioning.

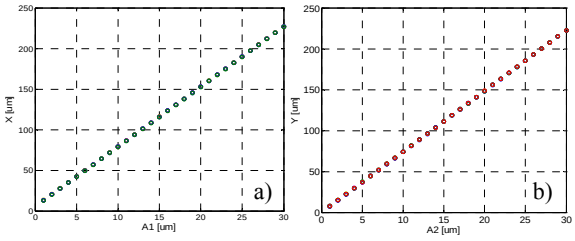

Figure 7: Experimental results of the range of motion for axes: a) X actuated by actuator A1; b) Y actuated by A2.

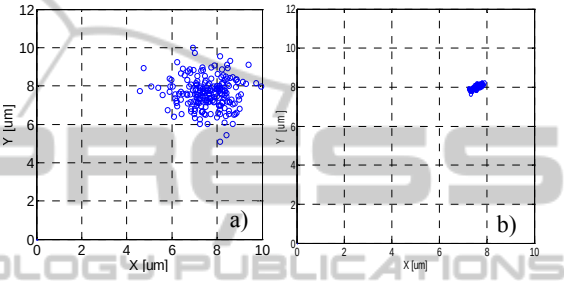

Figure 8: End-effector repeatability measurement: a) approach 1; b) approach 2.

An estimation of the manipulator mechanical parameters for different approaches is carried out. The performed experiments show that after system tensioning deflections arise from the starting position of the end-effector. At the first approach, these deflections are considerable, and at the second one they are smaller. At both approaches, the end-effector effective displacements at the same shifts of the actuators are equal.

Simulations of the manipulator with elastic joints are carried out using FEA based function of a CAD system. The simulations performed show that the motion of one axis interferes with the other axis and this influence is bigger at the first approach for pre-tensioning and smaller at the second one.

The proposed approaches for manipulator tensioning are experimented on the real manipulator prototype. Experimental investigation of the prototyped robotic system is realized by a digital image correlation technique. Obtained results of experiments testing of the prototyped micro-manipulator on the range of motion along the axes X and Y is $\chi_x = \chi_y = 226$ µm. The repeatability of the end-effector position is obtained for the case with open loop control system and without compensation of hysteresis. It was found for this case that maximal positioning error for the first approach is (3-5) µm and for the second one - (0-1) µm.

Further investigations and experiments are under

SCITEPRESS SCIENCE AND TECHNOLOGY PUBLICATIONS

consideration for closed loop control of the X and Y axes including hysteresis compensation method for piezo-actuators based on the discrete Preisach model (Marinov, 2009), as well as for injector pipette in Z-axis in order to realize the successful cell injection.

ACKNOWLEDGEMENTS

The authors gratefully acknowledge the support for this work through the project SpeSy-MiNT funded by the Bulgarian National Science Foundation under the Contract Nr. DO 0171/16.12.2008.

REFERENCES

Kasper, R. M.Al-Wahab, 2004. Mechanically Structured Piezoelectric Actuators, *9th Int. Conf. on New Actuators,* Bremen, Germany, pp.68-71.

Pernette, E, S. Henein, I. Magnani and R. Clavel, 1997. Design of Parallel Robots in Microrobotics, *Robotica*, vol.15, pp.417-420.

Yong, Y. K., Tien-Fu Lu, 2008. The Effect of the Accuracies of Flexure Hinge Equation on the Output Compliances of Planar Micro- motion Stages, *Mechanism and Machine Theory* 43, pp.347-363.

Chih-Liang Chu, Sheng-Hao Fan, 2006. A Novel Long-travel Piezoelectric- driven Linear Nanopositioning Stage, *Precision Engineering* 30, pp. 85-95.

Li Y. and Q. Xu, 2011. A Totally Decoupled Piezo-Driven XYZ Flexure Parallel Micropositioning Stage for Micro/Nanomanipulation, *IEEE Transactions On Automation Science And Engineering*, Vol. 8, No. 2.

Zhang, W., Zou, J., Watson, L., Zhao, W., 2002. The constant- jacobian method for kinematics of a three DOF planar micro-motion stage, *Journal of Robotic Systems 19(2)*, pp.63–72.

Pham, H., Chen, I., 2005. Stiffness modeling of flexure parallel mechanism, *Precision Engineering* 29, pp. 467–478.

Lu Z., X. Zhang, C. Leung, N. Esfandiari, R. Casper, Yu Sun, 2011. Robotic ICSI (Intracytoplasmic Sperm Injection), *IEEE Transactions on Biomedical Engineering,* vol. 58, No. 7, pp.2102-2108.

Tang, H., Y. Li, J. Huang, Q. Yang, 2012. Design and Assessment of a Flexure-Based 2-DOF Micromanipulator for Automatic Cell Micro-Injection, *Advanced Materials Res.*, vol. 457-458, pp. 445-448.

Chakarov, D., K. Kostadinov, T. Tiankov, 2009. Model and approaches for tension of parallel structures with elastic joints for micro and nano manipulators, *Int. Conf. on Informatics in Control, Automation and Robotics*, Milan, Italy, 2-5 July, Vol.2, pp.135-140.

Kostadinov, K., D. Chakarov, T. Tiankov, Fl. Ionescu, 2009. Robot for Micro and Nano Manipulations, *BG Patent*, Reg. No 110432/28.07.2009.

Liu, C., W. T. Freeman, R. Szleski, and S. B. Kang, 2006. "Noise Estimation from a single image", *IEEE Computer Vision and Pattern Recognition*, vol. 1, pp. 901-908.

Jin, H. and H. A. Bruck, 2005. Theoretical development for point wise digital image correlation, *Optical Engineering*, vol. 44, no. 1, pp. 1-14.

Shulev A., K. Kostadinov, T. Tiankov, and I. Roussev, 2011. Optical Positioning Control of a 3D Micro-manipulator, *Proceedings of 3M-NANO International Conference on Manipulation, Manufacturing and Measurement on the Nanoscale*, Changchun, China, 29.08-02.09.2011, paper 108, p.4.

Marinov M., 2009. "Method for Hysteresis Compensation in Piezo-actuators Using Discrete Preisah Model" *Journal Mechanics of the Machines, year XVII, vol. 80, ISSN, 0861-9727.*

SCITEPRESS SCIENCE AND TECHNOLOGY PUBLICATIONS